OPEN ACCESS Freely available online

PLOS ONE

Radiative Hydromagnetic Flow of Jeffrey Nanofluid by an Exponentially Stretching Sheet

Tariq Hussain[1]*, Sabir Ali Shehzad[2], Tasawar Hayat[2,3], Ahmed Alsaedi[3], Falleh Al-Solamy[3], Muhammad Ramzan[1]

1 Department of Mathematics, Faculty of Computing, Mohammad Ali Jinnah University, Islamabad Campus, Islamabad, Pakistan, **2** Department of Mathematics, Quaid-i-Azam University, Islamabad, Pakistan, **3** Nonlinear Analysis and Applied Mathematics (NAAM) Research Group, Faculty of Science, King Abdulaziz University, Jeddah, Saudi Arabia

Abstract

Two-dimensional hydromagnetic flow of an incompressible Jeffrey nanofluid over an exponentially stretching surface is examined in the present article. Heat and mass transfer analysis is performed in the presence of thermal radiation, viscous dissipation, and Brownian motion and thermophoresis effects. Mathematical modelling of considered flow problem is developed under boundary layer and Rosseland's approximations. The governing nonlinear partial differential equations are converted into ordinary differential equations via transformations. Solution expressions of velocity, temperature and concentration are presented in the series forms. Impacts of physical parameters on the dimensionless temperature and concentration are shown and discussed. Skin-friction coefficients are analyzed numerically. A comparison in a limiting sense is provided to validate the present series solutions.

Citation: Hussain T, Shehzad SA, Hayat T, Alsaedi A, Al-Solamy F, et al. (2014) Radiative Hydromagnetic Flow of Jeffrey Nanofluid by an Exponentially Stretching Sheet. PLoS ONE 9(8): e103719. doi:10.1371/journal.pone.0103719

Editor: Gongnan Xie, Northwestern Polytechnical University, China

Received March 16, 2014; **Accepted** July 4, 2014; **Published** August 1, 2014

Data Availability: The authors confirm that all data underlying the findings are fully available without restriction. All relevant data are within the paper and its Supporting Information files.

Funding: This project is funded by the Deanship of Scientific Research (DSR), King Abdulaziz University, Jeddah, Saudi Arabia under grant no. 37-130-35-HiCi. The authors, therefore, acknowledge with thanks DSR technical and financial support. The funders had no role in study design, data collection and analysis, decision to publish, or preparation of the manuscript.

Competing Interests: The authors have declared that no competing interests exist.

* Email: zartotariq@yahoo.com

Introduction

Boundary layer flow over a stretched surface is a subject of abundant studies now a days because of its existence in various engineering and industrial processes like cooling of metallic sheets in a cooling bath, annealing and thinning of copper wires, aerodynamic extrusion of plastic and rubber sheets, drawing of plastic films and sheets, glass fiber and paper production etc. It is worthmentioning to point out here that the stretching velocity is not linear necessarily in all the cases. The stretching velocity may be nonlinear or exponential. For example in annealing and thinning of copper wires, the desired quality product depends on the continuous stretching of surface with exponential dependence velocity distribution [1–6]. The magnetohydrodynamic flow is quite interesting in engineering and industrial processes. El Koumy et al. [7] investigated peristaltic flow of Maxwell fluid through a porous medium in the presence of Hall effects. Hall currents and heat transfer analysis in peristaltic flow is performed by Abo-Eldahab et al. [8]. Effects of magnetic field and porous space in peristaltic flow of Maxwell fluid are examined by Mekheimer et al. [9]. Shehzad et al. [10] discussed the Joule heating and thermophoresis effects in MHD flow of Jeffrey fluid induced by a stretching sheet. An induced magnetic field and slip effects in peristaltic flow through a porous medium are described by Mekheimer et al. [11]. Recently, Hayat et al. [12] performed a study to analyze the effects of Hall current and Ohmic heating in peristaltic flow of non-Newtonian fluid.

A working fluid is involved in many engineering and industrial applications that are in flowing or stagnant state. This working fluid is used to transfer energy/heat from one position to the other. The adequate heat transfer performance has been a major issue for a long period. This issue can be resolved by using a new working fluid that has better thermal performance than the ordinary base liquids. Recently nanofluid is the best candidate to take place of working fluid. Nanofluid is a fluid in which the nanoparticles are submerged. The size of these nanoparticles is 1–100 nm. The thermal conductivity of the nanofluids is higher than that of base fluids. Further, the novel properties of Brownian motion and thermophoresis of such fluids make them potentially useful. Nanoparticles are used to enhance the thermal characteristics of ordinary base fluids such as water, ethylene glycol or oil [13]. In addition the magneto-nanofluid is a unique material that has both liquid and magnetic properties. Such nanofluid has superficial role in construction of loud speakers, blood analysis and cancer therapy. Buongiorno [14] provided a mathematical model of nanofluid which has the characteristics of thermophoresis and Brownian motion. Later on, Makinde and Aziz [15] investigated the boundary layer flow of viscous nanofluid with convective thermal boundary condition. Here, the flow is induced due to linear stretching of surface. Closed form solutions of MHD nanofluid flow with heat and mass transfer analysis in the presence

of slip condition were developed by Turkyilmazoglu [16]. Ibrahim and Makinde [17] analyzed the effects of thermal and concentration stratifications in boundary layer nanofluid flow by a vertical surface. Second law of thermodynamics in MHD steady flow of nanofluid over a rotating disk was discussed by Rashidi et al. [18]. Moradi et al. [19] presented the series solutions of Jeffrey Hamel flow by considering the different types of nanoparticles. Unsteady natural convection flow of nanofluid with heat and mass transfer over a vertical plate was examined by Turkyilmazoglu and Pop [20]. Slip and Joule heating effects in MHD peristaltic flow of nanofluid under thermal diffusion and diffusion thermo effects was studied by Hayat et al. [21]. Sheikholeslami et al. [22] carried out an analysis to discuss the effects of an applied magnetic field in rotating flow of nanofluid with heat transfer.

The aim of present article is to study the flow analysis of Jeffrey fluid [23–28] in the presence of thermophoresis, Brownian motion, thermal radiation and viscous dissipation effects. The flow caused is by an exponentially stretching sheet. Jeffrey fluid has ability to exhibit the properties of ratio of stress relaxation to retardation and retardation. Mathematical formulation is performed under boundary layer and Rosseland's assumptions. Homotopy analysis method (HAM) [29–35] is utilized for solution expressions of dimensionless velocity, temperature and concentration. Temperature and concentration fields are shown and discussed for the different values of arising parameters. Skin-friction coefficients are computed and analyzed. Comparison of local Nusselt number in a limiting sense is tabulated and analyzed.

Mathematical Model

We consider the two-dimensional hydromagnetic flow of Jeffrey nanofluid over an exponentially stretching sheet. Heat and mass transfer effects are taken into account. An applied magnetic field of strength B_0 is encountered normal to the flow direction. The magnetic Reynolds number is chosen small and the Joule heating effects are absent. Further the induced magnetic field is smaller in comparison to the applied magnetic field and is negligible. In addition, viscous dissipation effects are also taken into account. The two-dimensional boundary layer equations of an incompressible Jeffrey nanofluid with heat and mass transfer are given below:

$$\frac{\partial u}{\partial x}+\frac{\partial v}{\partial y}=0, \tag{1}$$

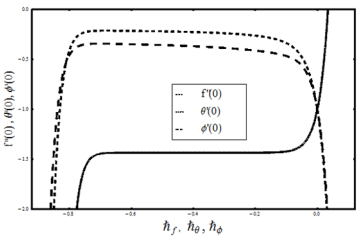

Figure 1. $\hbar$ − curves for functions $f(\eta)$, $\theta(\eta)$ and $\phi(\eta)$ at 21th order of approximations when $\lambda_1 = 0.3, \beta = 0.2, M = 0.5$, Pr = 0.7, $Le = 1.0$, $Nt = 0.2 = Nb$, $Ec = 0.3 = Rd$, $A = 0.1$ and $B = 0.2$.
doi:10.1371/journal.pone.0103719.g001

$$u\frac{\partial u}{\partial x}+v\frac{\partial u}{\partial y}=\frac{\nu}{1+\lambda_1}\left(\frac{\partial^2 u}{\partial y^2}+\lambda_2\left(\frac{\partial u}{\partial y}\frac{\partial^2 u}{\partial x\partial y}+u\frac{\partial^3 u}{\partial x\partial y^2}-\frac{\partial u}{\partial x}\frac{\partial^2 u}{\partial y^2}+v\frac{\partial^3 u}{\partial y^3}\right)\right)-\frac{\sigma B_0^2}{\rho_f}u, \tag{2}$$

$$u\frac{\partial T}{\partial x}+v\frac{\partial T}{\partial y}=\alpha\frac{\partial^2 T}{\partial y^2}+\tau\left(D_B\frac{\partial C}{\partial y}\frac{\partial T}{\partial y}+\frac{D_T}{T_\infty}\left(\frac{\partial T}{\partial y}\right)^2\right)+\frac{\nu}{c_p(1+\lambda_1)}\left(\frac{\partial u}{\partial y}\right)^2+\frac{\nu\lambda_2}{c_p(1+\lambda_1)}\frac{\partial u}{\partial y}\frac{\partial}{\partial y}\left(u\frac{\partial u}{\partial x}+v\frac{\partial u}{\partial y}\right)-\frac{1}{(\rho c)_p}\frac{\partial q_r}{\partial y}, \tag{3}$$

$$u\frac{\partial C}{\partial x}+v\frac{\partial C}{\partial y}=D_B\frac{\partial^2 C}{\partial y^2}+\frac{D_T}{T_\infty}\frac{\partial^2 T}{\partial y^2}, \tag{4}$$

The boundary conditions for the considered flow analysis are

$$u=U_w(x)=U_0\exp\left(\frac{x}{l}\right),\ v=0,\ T=T_w=T_\infty+T_0\exp\left(\frac{Ax}{l}\right),\quad C=C_w=C_\infty+C_0\exp\left(\frac{Bx}{l}\right)\ \text{ at } y=0, \tag{5}$$

Table 1. Convergence of homotopy solution for different order of approximations when $\lambda_1 = 0.3$, $\beta = 0.2$, $M = 0.5$, Pr $= 0.7 = Le$, $N_t = N_b = 0.2$, $Ec = 0.3 = Rd$, $A = 0.1$, $B = 0.2$ and $\hbar_f = -0.5 = \hbar_\theta = \hbar_\phi$.

Order of approximation	$-f''(0)$	$-\theta'(0)$	$-\phi'(0)$
1	1.2900	0.5316	0.5572
5	1.4310	0.2972	0.3806
11	1.4350	0.2433	0.3146
20	1.4350	0.2210	0.2692
30	1.4350	0.2124	0.2435
45	1.4350	0.2076	0.2225
50	1.4350	0.2076	0.2193
60	1.4350	0.2076	0.2193

doi:10.1371/journal.pone.0103719.t001

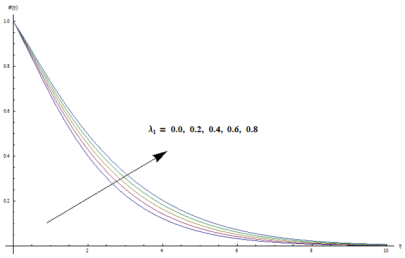

Figure 2. Variation in dimensionless temperature $\theta(\eta)$ vs η for different values of λ_1 when $\beta = 0.2$, $M = 0.5$, $\Pr = 0.7$, $Le = 1.0$, $Nt = 0.2 = Nb$, $Ec = 0.3 = Rd$, $A = 0.1$ and $B = 0.2$.
doi:10.1371/journal.pone.0103719.g002

$$u \to 0,\ T \to T_\infty,\ C \to C_\infty,\ \text{when}\ y \to \infty \tag{6}$$

where u and v are the velocity components in the $x-$ and $y-$ directions, ν the kinematic viscosity, λ_1 the ratio of relaxation to retardation times, λ_2 the relaxation time, ρ_f the density of fluid, σ the Steffan-Boltzman constant, α the thermal diffusivity, $\tau = \dfrac{(\rho c)_p}{(\rho c)_f}$ the ratio of nanoparticle heat capacity and the base fluid heat capacity, D_B the Brownian diffusion coefficient, D_T the thermophoretic diffusion coefficient, q_r the radiative heat flux, T_∞ and C_∞ are the ambient fluid temperature and concentration far away from the sheet and A, B, T_0, C_0 are the constants.

By employing Rosseland's approximation, Eq. (3) has the form

$$\begin{aligned} &u\frac{\partial T}{\partial x} + v\frac{\partial T}{\partial y} = \\ &\alpha + \frac{16\sigma^* T_\infty^3}{3k^*(\rho c)_p}\frac{\partial^2 T}{\partial y^2} + \tau\left(D_B\frac{\partial C}{\partial y}\frac{\partial T}{\partial y} + \frac{D_T}{T_\infty}\left(\frac{\partial T}{\partial y}\right)^2\right) \\ &+ \frac{\nu}{c_p(1+\lambda_1)}\left(\frac{\partial u}{\partial y}\right)^2 + \frac{\nu\lambda_2}{c_p(1+\lambda_1)}\frac{\partial u}{\partial y}\frac{\partial}{\partial y}\left(u\frac{\partial u}{\partial x} + v\frac{\partial u}{\partial y}\right), \end{aligned} \tag{7}$$

The dimensionless variables are defined as

$$\begin{aligned} &u = U_0 \exp\left(\frac{x}{l}\right) f'(\eta),\ v = -\sqrt{\frac{\nu U_0}{2l}}\exp\left(\frac{x}{2l}\right)(f(\eta) + \eta f'(\eta)), \\ &\eta = y\sqrt{\frac{U_0}{2\nu l}}\exp\left(\frac{x}{2l}\right),\ T = T_\infty + T_0 \exp\left(\frac{Ax}{2l}\right)\theta(\eta), \\ &C = C_\infty + C_0 \exp\left(\frac{Bx}{2l}\right)\phi(\eta). \end{aligned} \tag{8}$$

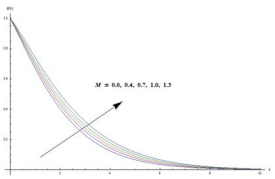

Figure 3. Variation in dimensionless temperature $\theta(\eta)$ vs η for different values of M when $\lambda_1 = 0.3$, $\beta = 0.2$, $\Pr = 0.7$, $Le = 1.0$, $Nt = 0.2 = Nb$, $Ec = 0.3 = Rd$, $A = 0.1$ and $B = 0.2$.
doi:10.1371/journal.pone.0103719.g003

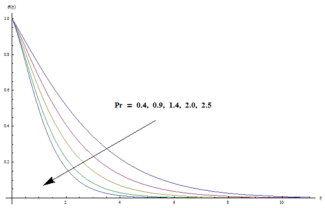

Figure 4. Variation in dimensionless temperature $\theta(\eta)$ vs η for different values of $\Pr$ when $\lambda_1 = 0.3$, $\beta = 0.2$, $M = 0.5$, $Le = 1.0$, $Nt = 0.2 = Nb$, $Ec = 0.3 = Rd$, $A = 0.1$ and $B = 0.2$.
doi:10.1371/journal.pone.0103719.g004

The equations of linear momentum, energy, concentration and their corresponding boundary conditions in dimensionless form can be written as

$$\begin{aligned} &f''' + (1+\lambda_1)ff'' - 2(1+\lambda_1)f'^2 + \beta\left(\frac{3}{2}f'^2 - \frac{1}{2}ff'''' + f'f'''\right) \\ &- M(1+\lambda_1)f' = 0, \end{aligned} \tag{9}$$

$$\begin{aligned} &(1+\lambda_1)\left(1+\frac{4}{3}Rd\right)\theta'' + \\ &(1+\lambda_1)\Pr(f\theta' - Af'\theta) + (1+\lambda_1)\Pr Nb\theta'\phi' \end{aligned}$$

$$+(1+\lambda_1)\Pr Nt\theta'^2 + \Pr Ec\left(f''^2 + \frac{\beta}{2}f''(3f'f'' - ff''')\right) = 0, \tag{10}$$

$$\phi'' + \Pr Le(f\phi' - Bf'\phi) + (N_t/N_b)\theta'' = 0, \tag{11}$$

$$f = 0, f' = 1, \theta' = 1, \phi' = 1 \text{ at } \eta = 0,$$

$$f' \to 0, \theta \to 0, \phi \to 0 \text{ as } \eta \to \infty, \tag{12}$$

where $\beta = \dfrac{\lambda_2 U_0 \exp\left(\frac{x}{l}\right)}{l}$ is the Deborah number, $M = \dfrac{\sigma B_0^2 U_w}{\rho_f c}$ is the magnetic parameter, $\Pr = \dfrac{\nu}{\alpha}$ is the Prandtl number, $Ec = \dfrac{U_0^2}{c_p T_0}\left(\dfrac{U_w}{U_0}\right)\left(\dfrac{4-A}{2}\right)$ is the Eckert number,

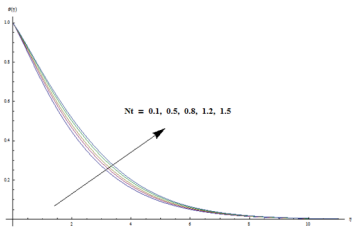

Figure 5. Variation in dimensionless temperature $\theta(\eta)$ vs η for different values of Nt when $\lambda_1 = 0.3$, $\beta = 0.2$, $M = 0.5$, $\Pr = 0.7$, $Le = 1.0$, $Nb = 0.2$, $Ec = 0.3 = Rd$, $A = 0.1$ and $B = 0.2$.
doi:10.1371/journal.pone.0103719.g005

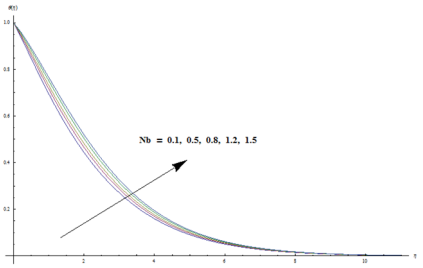

Figure 6. Variation in dimensionless temperature $\theta(\eta)$ vs η for different values of Nb when $\lambda_1 = 0.3$, $\beta = 0.2$, $M = 0.5$, $\Pr = 0.7$, $Le = 1.0$, $Nt = 0.2$, $Ec = 0.3 = Rd$, $A = 0.1$ and $B = 0.2$. doi:10.1371/journal.pone.0103719.g006

$Le = \dfrac{\alpha}{D_B}$ is the Lewis number, $Nb = \dfrac{(\rho c)_p D_B C_0 \exp\left(\dfrac{Bx}{2l}\right)}{(\rho c)_f \nu}$ is the Brownian motion parameter, $Nt = \dfrac{(\rho c)_p D_T T_0 \exp\left(\dfrac{Ax}{2l}\right)}{(\rho c)_f \nu T_\infty}$ is the thermophoresis parameter,

The skin friction coefficient, the local Nusselt and Sherwood numbers are defined below.

$$C_f = \frac{\tau_w}{\rho_f U_w^2(x)}, Nu_x = \frac{x q_w}{k(T_w - T_\infty)}, Sh_x = \frac{x q_m}{D_B(C_w - C_\infty)}, \quad (13)$$

where τ_w is the shear stress along the stretching surface, q_w is the surface heat flux and q_m is the surface mass flux. The local skin-friction coefficient, local Nusselt and Sherwood numbers in dimensionless forms can be written as

$$\sqrt{2\mathrm{Re}_x} C_{fx} = \frac{1}{1+\lambda_1}(f''(0) + \beta f''(0)), Nu_x/\mathrm{Re}_x^{1/2} = -\sqrt{\frac{x}{2l}}\left(1 + \frac{4}{3}Rd\right)\theta'(0), \quad (14)$$

$$Sh_x/\mathrm{Re}_x^{1/2} = -\sqrt{\frac{x}{2l}}\phi'(0),$$

where $\mathrm{Re}_x = U_w(x)x/\nu$ is the local Reynolds number.

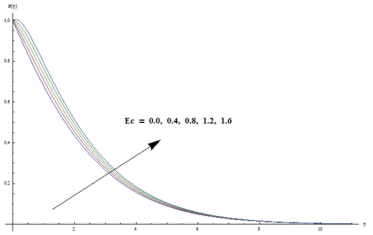

Figure 7. Variation in dimensionless temperature $\theta(\eta)$ vs η for different values of Ec when $\lambda_1 = 0.3$, $\beta = 0.2$, $M = 0.5$, $\Pr = 0.7$, $Le = 1.0$, $Nt = 0.2 = Nb$, $Rd = 0.3$, $A = 0.1$ and $B = 0.2$. doi:10.1371/journal.pone.0103719.g007

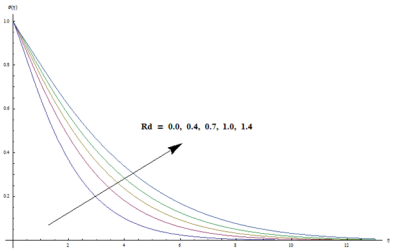

Figure 8. Variation in dimensionless temperature $\theta(\eta)$ vs η for different values of Rd when $\lambda_1 = 0.3$, $\beta = 0.2$, $M = 0.5$, $\Pr = 0.7$, $Le = 1.0$, $Nt = 0.2 = Nb$, $Ec = 0.3$, $A = 0.1$ and $B = 0.2$. doi:10.1371/journal.pone.0103719.g008

Homotopy Analysis Solutions

To proceed the homotopic solutions, the initial guesses and auxiliary linear operators are chosen as follows:

$$f_0(\eta) = 1 - \exp(-\eta), \theta_0(\eta) = \exp(-\eta), \phi_0(\eta) = \exp(-\eta), \quad (15)$$

$$L(f) = f''' - f', L(\theta) = \theta'' - \theta, L(\phi) = \phi'' - \phi. \quad (16)$$

The above initial guesses and auxiliary linear operators satisfies the below mentioned properties

$$\begin{aligned} L(f)(C_1 + C_2 e^{\eta} + C_3 e^{-\eta}) &= 0, \\ L(\theta)(C_4 e^{\eta} + C_5 e^{-\eta}) &= 0, \\ L(\phi)(C_6 e^{\eta} + C_7 e^{-\eta}) &= 0, \end{aligned} \quad (17)$$

where $C_i (\, i = 1 - 7)$ are the arbitrary constants.

The zeroth order problems can be written as

$$(1-q)L(f)\left[\bar{f}(\eta; q) - f_0(\eta)\right] = q\hbar_f \mathbf{N}_f\left[\bar{f}(\eta; q)\right], \quad (18)$$

$$(1-q)L(\theta)\left[\bar{\theta}(\eta; q) - \theta_0(\eta)\right] = q\hbar_\theta \mathbf{N}_\theta\left[\bar{f}(\eta; q), \bar{\theta}(\eta, q), \bar{\phi}(\eta, q)\right], \quad (19)$$

$$(1-q)L(\phi)\left[\bar{\phi}(\eta; q) - \theta_0(\eta)\right] = q\hbar_\theta \mathbf{N}_\theta\left[\bar{f}(\eta; q), \bar{\theta}(\eta, q), \bar{\phi}(\eta, q)\right], \quad (20)$$

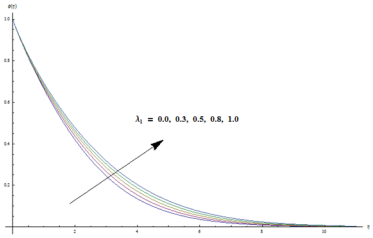

Figure 9. Variation in dimensionless concentration $\phi(\eta)$ vs η for different values of λ_1 when $\beta = 0.2$, $M = 0.5$, $\Pr = 0.7$, $Le = 1.0$, $Nt = 0.2 = Nb$, $Rd = 0.3 = Ec$, $A = 0.1$ and $B = 0.2$. doi:10.1371/journal.pone.0103719.g009

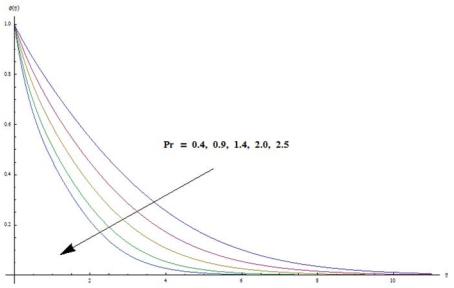

Figure 10. Variation in dimensionless concentration $\phi(\eta)$ vs η for different values of Pr when $\lambda_1 = 0.3$, $\beta = 0.2$, $M = 0.5$, $Le = 1.0$, $Nt = 0.2 = Nb$, $Rd = 0.3 = Ec$, $A = 0.1$ and $B = 0.2$. doi:10.1371/journal.pone.0103719.g010

$$\begin{aligned}&\bar{f}(0;\,q)=0,\bar{f}'(0;\,q)=1,\bar{\theta}(0,q)\\&=-Bi_1(1-\bar{\theta}(0,q)),\bar{\phi}'(0,q)\\&=-Bi_2(1-\bar{\phi}(0,q)),\end{aligned}$$

$$\bar{f}'(\infty;\,q)=0,\bar{\theta}(\infty,q)=0,\bar{\phi}(\infty,q)=0, \tag{21}$$

$$\begin{aligned}N_f[\bar{f}(\eta,q)]=&\frac{\partial^3\bar{f}(\eta,q)}{\partial\eta^3}+(1+\lambda_1)\left(\hat{f}(\eta,q)\frac{\partial^2\hat{f}(\eta,q)}{\partial\eta^2}\right)\\&-2(1+\lambda_1)\left(\frac{\partial\hat{f}(\eta,q)}{\partial\eta}\right)^2\\&+\beta\left(\begin{array}{l}\frac{3}{2}\left(\frac{\partial^2\hat{f}(\eta,q)}{\partial\eta^2}\right)^2\\-\frac{1}{2}\hat{f}(\eta,q)\frac{\partial^4\hat{f}(\eta,q)}{\partial\eta^4}+\frac{\partial\hat{f}(\eta,q)}{\partial\eta}\frac{\partial^3\hat{f}(\eta,q)}{\partial\eta^3}\end{array}\right)\\&-(1+\lambda_1)M\frac{\partial\bar{f}(\eta,q)}{\partial\eta},\end{aligned} \tag{22}$$

$$\begin{aligned}&\mathbf{N}_\theta[\bar{\theta}(\eta,q),\bar{f}(\eta,q),\bar{\phi}(\eta,q)]=\\&(1+\lambda_1)\left(1+\frac{4}{3}Rd\right)\frac{\partial^2\bar{\theta}(\eta,q)}{\partial\eta^2}+(1+\lambda_1)\Pr N_b\frac{\partial\bar{\theta}(\eta,q)}{\partial\eta}\frac{\partial\bar{\phi}(\eta,q)}{\partial\eta}\\&(1+\lambda_1)\Pr\left(\frac{\partial\bar{\theta}(\eta,q)}{\partial\eta}\hat{f}(\eta,q)-A\frac{\partial\hat{f}(\eta,q)}{\partial\eta}\bar{\theta}(\eta,q)\right)\\&+(1+\lambda_1)\Pr N_t\left(\frac{\partial\bar{\theta}(\eta,q)}{\partial\eta}\right)^2+\Pr Ec\left(\frac{\partial^2\hat{f}(\eta,q)}{\partial\eta^2}\right)^2\\&+\frac{\Pr Ec\beta}{2}\left(3\frac{\partial\hat{f}(\eta,q)}{\partial\eta}\frac{\partial^2\hat{f}(\eta,q)}{\partial\eta^2}-\hat{f}(\eta,q)\frac{\partial^2\hat{f}(\eta,q)}{\partial\eta^2}\right),\end{aligned} \tag{23}$$

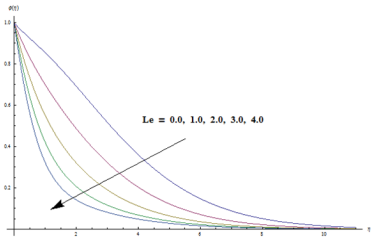

Figure 11. Variation in dimensionless concentration $\phi(\eta)$ vs η for different values of Le when $\lambda_1 = 0.3$, $\beta = 0.2$, $M = 0.5$, Pr $= 0.7$, $Nt = 0.2 = Nb$, $Rd = 0.3 = Ec$, $A = 0.1o$ and $B = 0.2$. doi:10.1371/journal.pone.0103719.g011

$$\begin{aligned}N_\phi[\bar{\phi}(\eta,q),\bar{f}(\eta,q),\bar{\theta}(\eta,q)]=&\frac{\partial^2\bar{\phi}(\eta,q)}{\partial\eta^2}+\\&\Pr Le\left(\bar{f}(\eta,q)\frac{\partial\bar{\phi}(\eta,q)}{\partial\eta}-B\frac{\partial\hat{f}(\eta,q)}{\partial\eta}\bar{\phi}(\eta,q)\right)+\\&(N_t/N_b)\frac{\partial^2\bar{\theta}(\eta,q)}{\partial\eta^2},\end{aligned} \tag{24}$$

where $\hbar_f$, $\hbar_\theta$ and $\hbar_\phi$ are the non-zero auxiliary parameters, $q \in [0,\ 1]$ is an embedding parameter and $\mathbf{N}_f$, $\mathbf{N}_\theta$ and $\mathbf{N}_\phi$ are the nonlinear operators. Putting $q = 0$ and $q = 1$ one has

$$\begin{aligned}&\bar{f}(\eta;\,0)=f_0(\eta),\bar{\theta}(\eta,0)=\theta_0(\eta),\bar{\phi}(\eta,0)=\phi_0(\eta)\text{ and }\bar{f}(\eta;\,1)=f(\eta),\\&\bar{\theta}(\eta,1)=\theta(\eta),\bar{\phi}(\eta,1)=\phi(\eta).\end{aligned} \tag{25}$$

When we increase the values of q from 0 to 1 then $f(\eta, q)$, $\theta(\eta, q)$ and $\phi(\eta, q)$ vary from $f_0(\eta)$, $\theta_0(\eta)$, $\phi_0(\eta)$ to $f(\eta)$, $\theta(\eta)$ and $\phi(\eta)$. By adopting Taylor series expansion, we have [28–30]:

$$f(\eta,q)=f_0(\eta)+\sum_{m=1}^{\infty}f_m(\eta)q^m, \tag{26}$$

$$\theta(\eta,q)=\theta_0(\eta)+\sum_{m=1}^{\infty}\theta_m(\eta)q^m, \tag{27}$$

$$\phi(\eta,q)=\phi_0(\eta)+\sum_{m=1}^{\infty}\phi_m(\eta)q^m, \tag{28}$$

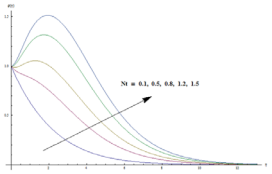

Figure 12. Variation in dimensionless concentration $\phi(\eta)$ vs η for different values of Nt when $\lambda_1 = 0.3$, $\beta = 0.2$, $M = 0.5$, Pr $= 0.7$, $Le = 1.0$, $Nb = 0.2$, $Rd = 0.3 = Ec$, $A = 0.1$ and $B = 0.2$. doi:10.1371/journal.pone.0103719.g012

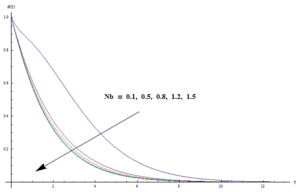

Figure 13. Variation in dimensionless concentration $\phi(\eta)$ vs η for different values of Nt when $\lambda_1 = 0.3$, $\beta = 0.2$, $M = 0.5$, $\Pr = 0.7$, $Le = 1.0$, $Nt = 0.2$, $Rd = 0.3 = Ec$, $A = 0.1$ and $B = 0.2$.
doi:10.1371/journal.pone.0103719.g013

$$f_m(\eta) = \frac{1}{m!}\frac{\partial^m f(\eta;\, q)}{\partial \eta^m}\bigg|_{q=0}, \quad \theta_m(\eta) = \frac{1}{m!}\frac{\partial^m \theta(\eta;\, q)}{\partial \eta^m}\bigg|_{q=0}, \quad \phi_m(\eta) = \frac{1}{m!}\frac{\partial^m \phi(\eta;\, q)}{\partial \eta^m}\bigg|_{q=0}. \tag{29}$$

The convergence of above series highly depends upon the suitable values of $\hbar_f$, $\hbar_\theta$ and $\hbar_\vartheta$. Considering that $\hbar_f$, $\hbar_\theta$ and $\hbar_\vartheta$ are selected properly such that (26)–(28) converge at $q = 1$ and then we have

$$f(\eta) = f_0(\eta) + \sum_{m=1}^{\infty} f_m(\eta), \tag{30}$$

$$\theta(\eta) = \theta_0(\eta) + \sum_{m=1}^{\infty} \theta_m(\eta), \tag{31}$$

$$\phi(\eta) = \phi_0(\eta) + \sum_{m=1}^{\infty} \phi_m(\eta). \tag{32}$$

The general solutions can be written as

$$f_m(\eta) = f_m^*(\eta) + C_1 + C_2 e^{\eta} + C_3 e^{-\eta}, \tag{33}$$

$$\theta_m(\eta) = \theta_m^*(\eta) + C_4 e^{\eta} + C_5 e^{-\eta}, \tag{34}$$

$$\phi_m(\eta) = \phi_m^*(\eta) + C_6 e^{\eta} + C_7 e^{-\eta}, \tag{35}$$

where $f_m^*(\eta)$, $\theta_m^*(\eta)$ and $\phi_m^*(\eta)$ are the special solutions.

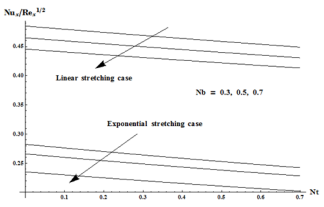

Figure 14. Variation in Nusselt and Sherwood numbers for different values of Nb vs Nt when $\lambda_1 = 0.3$, $\beta = 0.2$, $M = 0.5$, $\Pr = 0.7$, $Le = 1.0$, $Rd = 0.3 = Ec$, $A = 0.1$ and $B = 0.2$.
doi:10.1371/journal.pone.0103719.g014

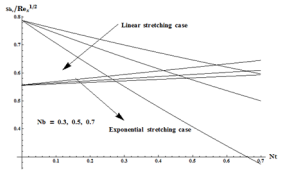

Figure 15. Variation in Nusselt and Sherwood numbers for different values of Nb vs Nt when $\lambda_1 = 0.3$, $\beta = 0.2$, $M = 0.5$, $\Pr = 0.7$, $Le = 1.0$, $Nt = 0.2$, $Rd = 0.3 = Ec$, $A = 0.1$ and $B = 0.2$.
doi:10.1371/journal.pone.0103719.g015

Convergence Analysis and Discussion

The auxiliary parameters $\hbar_f$, $\hbar_\theta$ and $\hbar_\vartheta$ are encountered when homotopy analysis method has been utilized to compute the series solutions. These parameters have essential importance for adjusting and controlling the convergence of series solutions. The appropriate values of these parameters are required for the convergent solutions. To obtain the proper values of these auxiliary parameters, we drawn the $\hbar$ − curves at 21^{th} -order of HAM approximations. These $\hbar$ − curves are presented in Fig. 1. From this Fig. we examined that the suitable values of $\hbar_f$, $\hbar_\theta$ and $\hbar_\vartheta$ are $-0.65 \le \hbar_f \le -0.10$, $-0.70 \le \hbar_\theta \le -0.30$, $-65 \le \hbar_\phi \le -0.30$. The series converges in the whole region of η when $\hbar_f = -0.5 = \hbar_\theta = \hbar_\phi$ (see Table 1).

Figs. 2–8 are drawn to examine the variations in dimensionless temperature profile $\theta(\eta)$ for different values of ratio of relaxation to retardation times λ_1, magnetic parameter M, Prandtl number $\Pr$, thermophoresis parameter Nt, Brownian motion parameter Nb, Eckert number Ec and radiation parameter Rd. Fig. 2 shows that an increase in ratio of relaxation to retardation times gives rise to the temperature and thermal boundary layer thickness. Minimum temperature and thinnest thermal boundary layer thickness is noticed when $\lambda_1 = 0$. An increase in λ_1 implies to an increase in relaxation time and decrease in retardation time. This change in relaxation and retardation times elucidates the higher temperature and thicker thermal boundary layer thickness. Change in temperature profile for different values of magnetic parameter is noticed in Fig. 3. Here we examined that both temperature and thermal boundary layer thickness are enhanced for larger magnetic parameter. It is also seen that for $M = 0$, hydrodynamic flow situation is recovered. Magnetic parameter involves the Lorentz force. Higher magnetic parameter implies to stronger Lorentz force and lower magnetic parameter has weaker Lorentz force. Here the stronger Lorentz force leads to an increase in the temperature and thermal boundary layer thickness. Fig. 4 depicts the impact of Prandtl number on the temperature field. It is observed that lower temperature and thinner thermal boundary layer thickness appear corresponding to the increasing values of Prandtl number. Prandtl number is the ratio of viscous to thermal diffusivities. Larger Prandtl number fluids have higher viscous diffusivity and weaker thermal diffusivity. Such change in viscous and thermal diffusivities leads to a decrease in thermal boundary layer thickness. Figs. 5 and 6 illustrate that both temperature and thermal boundary layer thickness are enhanced when the larger values of thermophoresis and Brownian motion parameters are taken into account. From Fig. 7 we noticed that temperature is an increasing function of Eckert number. Further $Ec = 0$ corresponds to the analysis when viscous dissipation effects are absent. Effects of radiative parameter on the temperature field are analyzed in Fig. 8. We observed that an increase in radiative parameter leads

Table 2. Numerical values of skin friction coefficient $\sqrt{2Re}C_{fx}$ for different values of λ_1, M and β in case of exponential and linear stretching.

λ_1	M	β	$-\sqrt{2Re}C_{fx}$	$-\sqrt{2Re}\,C_{fx}$
			Exponential stretching case	**Linear stretching case**
0.0	0.5	0.2	1.63612	1.34164
0.4			1.38278	1.13389
0.7			1.25485	1.02899
1.0			1.15689	0.94868
0.3	0.0	0.2	1.25661	0.96077
	0.7		1.50007	1.25269
	1.0		1.59258	1.35873
	1.4		1.70796	1.48842
0.3	0.5	0.0	1.28616	1.07417
		0.3	1.50353	1.22474
		0.5	1.63159	1.31559
		0.8	1.80611	1.44115

doi:10.1371/journal.pone.0103719.t002

to an enhancement in the temperature field. In fact an increase in radiative parameter provides more heat to fluid that corresponds to higher temperature.

Change in concentration distribution function $\phi(\eta)$ for various values of ratio of relaxation to retardation times λ_1, Prandtl number $\Pr$, Lewis number Le, thermophoresis parameter Nt and Brownian motion parameter Nb is examined through the Figs. 9–13. Fig. 9 clearly indicates that concentration and its related boundary layer thickness are increasing functions of ratio of relaxation to retardation times. In addition a comparison of the Figs. 2 and 9 shows that the impacts of ratio of relaxation to retardation times on the temperature and concentration are quite reverse. Fig. 10 depicts that concentration boundary layer thickness become thinner for larger Prandtl number. Form Fig. 11 we noticed that an increase in Lewis number shows lower concentration field. Lewis number is inversely proportional to the Brownian diffusion coefficient. This Brownian diffusion coefficient becomes smaller corresponding to the larger values of Lewis number. This smaller Brownian diffusion coefficient shows a reduction in the concentration and associated boundary layer thickness. Fig. 12 presents that the larger values of thermophoresis parameter give rise to the concentration and its related boundary layer thickness. It is also seen that concentration is at the peak when $Nt = 1.5$ and $\eta = 2.0$. Fig. 13 is drawn to see the variations in concentration profile when $Nb = 0.1,\ 0.5,\ 0.8,\ 1.2$ and 1.5. We have seen that the concentration and its related boundary layer thickness is decreased by increasing the Brownian motion parameter. It is also observed that the concentration profile decreases rapidly when $Nt = 0.1$ but after $Nt = 0.5$ this reduction is very small (see Fig. 13). Figs. 14 and 15 are drawn to examine

Table 3. Comparison values of $-\theta'(0)$ with Bidin and Nazar [3] for different values of Ec, $\Pr$ and Rd when $\beta = 0$, $\lambda_1 = 0$, $M = 0$, $Nt = Nb = 0$, $A = 1.0$ and $\hbar_\theta = -0.5$..

Rd	**Bidin and Nazar [3]**			**Present HAM solutions**		
	Ec = 0.0			***Ec = 0.0***		
	Pr = 1.0	***Pr = 2.0***	***Pr = 3.0***	***Pr = 1.0***	***Pr = 2.0***	***Pr = 3.0***
0.0	0.955	1.471	1.869	0.9548	1.4715	1.8693
0.5	0.677	1.074	1.381	0.6775	1.0734	1.3807
1.0	0.532	0.863	1.121	0.5337	0.8627	1.1213
Rd	*Ec = 0.2*			*Ec = 0.2*		
	0.862	1.306	1.688	0.8624	1.3055	1.6384
	0.618	0.965	1.229	0.6183	0.9653	1.2286
	0.488	0.782	1.007	0.4889	0.7818	1.0067
Rd	*Ec = 0.9*			*Ec = 0.9*		
	0.539	0.725	0.830	0.5387	0.7248	0.8302
	0.410	0.587	0.696	0.4111	0.5870	0.6963
	0.334	0.498	0.606	0.3355	0.4984	0.6055

doi:10.1371/journal.pone.0103719.t003

the variations in Nusselt and Sherwood numbers for different values Nb vs Nt for both linear and exponential stretching cases. Here we noticed that heat and mass transfer rates at wall are higher for linear stretching case in comparison to exponential case.

Table 1 is computed to examine the values of $-f''(0)$, $-\theta'(0)$ and $-\phi'(0)$ when $\lambda_1 = 0.3$, $\beta = 0.2$, $M = 0.5$, $\Pr = 0.7 = Le$, $Nt = 0.2 = Nb$, $Ec = 0.3 = Rd$, $A = 0.1$, $B = 0.2$ and $\hbar_f = 0.5 = \hbar_\theta = \hbar_\phi$. From this Table, we analyzed that the values of $-f''(0)$ converge from 11th order of HAM approximations whereas the values of $-\theta'(0)$ and $-\phi'(0)$ converge from 45th and 50th order of HAM deformations, respectively. Numerical values of skin-friction coefficient $\sqrt{2Re}C_{fx}$ for different values of λ_1, M and β of both exponential stretching and linear stretching cases are presented in Table 2. Here we examined that the values of skin-friction coefficient are smaller for larger λ_1 while these values are increased when larger values of M and β are encountered. Further, it is noticed that the values of skin-friction coefficient are larger for exponential stretching case in comparison to the linear stretching case. Table 3 provides a comparison study with the existing solutions for different values of Rd, Ec and $\Pr$ when $A = B = 1.0$, $\lambda_1 = \beta = M = 0$. From this Table one can see that our present results have an excellent agreement with the results of Bidin and Nazar [3].

Conclusions

Radiative hydromagnetic flow of Jeffrey nanofluid over an exponentially stretching sheet is studied. Heat and mass transfer phenomena are discussed in the presence of viscous dissipation. The main observations of present investigation are written below:

- Temperature and concentration profiles are enhanced with an increase in the ratio of relaxation to retardation times.
- Larger values of Deborah number β correspond to a reduction in the temperature and concentration fields.
- Thermophoresis and Brownian motion parameters give rise to the temperature and thermal boundary layer thickness.
- Temperature and thermal boundary layer thickness are increasing functions of radiative parameter Rd and Eckert number Ec.
- Brownian motion parameter has reverse effects on temperature and concentration.
- Values of skin-friction coefficient are increased by increasing M and β but it decreases when we increase the values of λ_1.

Acknowledgments

We are grateful to the reviewers for the useful suggestions and comments. This project is funded by the Deanship of Scientific Research (DSR), King Abdulaziz University, Jeddah, Saudi Arabia under grant no. 37-130-35-HiCi. The authors, therefore, acknowledge with thanks DSR technical and financial support.

Author Contributions

Conceived and designed the experiments: T. Hussain SAS T. Hayat AA FA MR. Performed the experiments: T. Hussain SAS T. Hayat AA FA MR. Analyzed the data: T. Hussain SAS T. Hayat AA FA MR. Contributed reagents/materials/analysis tools: T. Hussain SAS T. Hayat AA FA MR. Contributed to the writing of the manuscript: T. Hussain SAS T. Hayat AA FA MR.

References

1. Bidin B, Nazar R (2009) Numerical solution of the boundary layer flow over an exponentially stretching sheet with thermal radiation. Europ J Scientific Research 33: 710–717.
2. Sahoo B, Poncet S (2011) Flow and heat transfer of a third grade fluid past an exponentially stretching sheet with partial slip boundary condition. Int J Heat Mass Transfer 54: 5010–5019.
3. Mukhopadhyay S (2013) Slip effects on MHD boundary layer flow over an exponentially stretching sheet with suction/blowing and thermal radiation. Ain Shams Eng J 4: 485–491.
4. Liu IC, Wang HH, Peng YF (2013) Flow and heat transfer for three-dimensional flow over an exponentially stretching surface. Chem Eng Commun 200: 253–268.
5. Jalil M, Asghar S (2013) Flow of power-law fluid over a stretching surface: A Lie group analysis. Int J Non-Linear Mech 48: 65–71.
6. Hayat T, Shehzad SA, Alsaedi A (2014) MHD three dimensional flow by an exponentially stretching surface with convective boundary condition. J Aerospace Eng DOI:10.1061/(ASCE)AS.1943-5525.0000360.
7. El Koumy SR, Barakat ESI, Abdelsalam SI (2012) Hall and porous boundaries effects on peristaltic transport through porous medium of a Maxwell model. Transp Porous Med 94: 643–658.
8. Abo-Eldahab E, Barakat E, Nowar Kh (2012) Hall currents and heat transfer effects on peristaltic transport in a vertical asymmetric channel through a porous medium. Math Problems Eng 2012: 840203.
9. Mekheimer KhS, Komy SR Abdelsalam (2013) Simultaneous effects of magnetic field and space porosity on compressible Maxwell fluid transport induced by a surface acoustic wave in a microchannel. Chin Phys B 22: 124702.
10. Shehzad SA, Alsaedi A, Hayat T (2013) Influence of thermophoresis and Joule heating on the radiative flow of Jeffrey fluid with mixed convection. Braz J Chem Eng 30: 897–908.
11. Mekheimer KhS, Salem AM, Zaher AZ (2014) Peristatcally induced MHD slip flow in a porous medium due to a surface acoustic wavy wall. J Egypt Math Soc 22: 143–151.
12. Hayat T, Abbasi FM, Alsaedi A, Alsaadi F (2014) Hall and Ohmic heating effects on the peristaltic transport of a Carreau-Yasuda fluid in an asymmetric channel. Z Naturforsch 68: 43–51.
13. Choi SUS (1995) Enhancing thermal conductivity of fluids with nanoparticles. ASME MD 231, FED 66: 99–105.
14. Buongiorno J (2006) Convective transport in nanofluids. J Heat Transfer 128: 240–250.
15. Makinde OD, Aziz A (2011) Boundary layer flow of a nanofluid past a stretching sheet with a convective boundary condition. Int J Thermal Sci 50: 1326–1332.
16. Turkyilmazoglu M (2012) Exact analytical solutions for heat and mass transfer of MHD slip flow in nanofluids. Chem Eng Sci 84: 182–187.
17. Ibrahim W, Makinde OD (2013) The effect of double stratification on boundary-layer flow and heat transfer of nanofluid over a vertical plate. Comput Fluids 86: 433–441.
18. Rashidi MM, Abelman S, Mehr NF (2013) Entropy generation in steady MHD flow due to a rotating porous disk in a nanofluid. Int J Heat Mass Transfer 62: 515–525.
19. Moradi A, Alsaedi A, Hayat T (2013) Investigation of nanoparticles effect on the Jeffery-Hamel flow. Arab J Sci Eng 38: 2845–2853.
20. Turkyilmazoglu M, Pop I (2013) Heat and mass transfer of unsteady natural convection flow of some nanofluids past a vertical infinite flat plate with radiation effect. Int J Heat Mass Transfer 59: 167–171.
21. Hayat T, Abbasi FM, Al-Yami M, Monaquel S (2014) Slip and Joule heating effects in mixed convection peristaltic transport of nanofluid with Soret and Dufour effects. J Molecu Liquids 194: 93–99.
22. Sheikholeslami M, Hatami M, Ganji DD (2014) Nanofluid flow and heat transfer in a rotating system in the presence of a magnetic field. J Molecu Liquids 190: 112–120.
23. Hayat T, Ahmad N, Ali N (2008) Effects of an endoscope and magnetic field on the peristalsis involving Jeffrey fluid. Commun Nonlinear Sci Numer Simulat 13: 1581–1591.
24. Nadeem S, Zaheer S, Fang T (2011) Effects of thermal radiation on the boundary layer flow of a Jeffrey fluid over an exponentially stretching surface. Numer Algorithms 57: 187–205.
25. Turkyilmazoglu M, Pop I (2013) Exact analytical solutions for the flow and heat transfer near the stagnation point on a stretching/shrinking sheet in a Jeffrey fluid. Int J Heat Mass Transfer 57: 82–88.
26. Hamad MAA, AbdEl-Gaied SM, Khan WA (2013) Thermal jump effects on boundary layer flow of a Jeffrey fluid near the stagnation point on a stretching/shrinking sheet with variable thermal conductivity. J Fluids 2013: 749271.
27. Shehzad SA, Alsaadi FE, Monaquel SJ, Hayat T (2013) Soret and Dufour effects on the stagnation point flow of Jeffery fluid with convective boundary conditions. Europ Phys J Plus 128: 56.
28. Mekheimer KhS, Hemada KA, Raslan KR, Abo-Elkhair RE, Moawad AMA (2014) Numerical study of a non-linear peristaltic transport: Application of Adomian decomposition method (ADM). Gen Math Notes 20: 22–49.
29. Liao SJ (2012) Homotopy analysis method in nonlinear differential equations. Springer & Higher Education Press, Heidelberg.
30. Turkyilmazoglu M (2012) Solution of the Thomas-Fermi equation with a convergent approach. Commun Nonlinear Sci Numer Simulat 17: 4097–4103.

31. Abbasbandy S, Hashemi MS, Hashim I (2013) On convergence of homotopy analysis method and its application to fractional integro-differential equations. Quaestiones Mathematicae 36: 93–105.
32. Shehzad SA, Alsaedi A, Hayat T (2013) Hydromagnetic steady flow of Maxwell fluid over a bidirectional stretching surface with prescribed surface temperature and prescribed surface heat flux. Plos One 8: 68139.
33. Rashidi MM, Rajvanshi SC, Kavyani N, Keimanesh M, Pop I, et al. (2014) Investigation of heat transfer in a porous annulus with pulsating pressure gradient by homotopy analysis method. Arab J Sci Eng in press.
34. Shehzad SA, Alsaedi A, Hayat T, Alhuthali MS (2013) Three-dimensional flow of an Oldroyd-B fluid with variable thermal conductivity and heat generation/absorption. Plos One 8: 78240.
35. Hayat T, Shehzad SA, Al-Mezel S, Alsaedi A (2014) Three-dimensional flow of an Oldroyd-B fluid over a bidirectional stretching surface with prescribed surface temperature and prescribed surface heat flux. J Hydrol Hydromech 62: 117–125.